REYNOLDS-AVERAGED NAVIER-STOKES SIMULATION AROUND MK 48 ADCAP TORPEDOES

by

Austen Suqi

A Thesis

Submitted to the Faculty of Purdue University

In Partial Fulfillment of the Requirements for the degree of

Master of Science in Mechanical Engineering

School of Mechanical Engineering

West Lafayette, Indiana

December 2021

THE PURDUE UNIVERSITY GRADUATE SCHOOL

STATEMENT OF COMMITTEE APPROVAL

Dr. Carlo Scalo, Chair

School of Mechanical Engineering

Dr. Luciano Castillo

School of Mechanical Engineering

Dr. Sally Bane

School of Aeronautics and Astronautics

Approved by:

Dr. Nicole L. Key

Dedicated to the United States Submarine Force.

ACKNOWLEDGMENTS

Thank you to Dr. Scalo for providing me the tools and guidance required to complete this work. I would also like to thank my fiancée Allison for all her support and patience during the long days and nights in front of my computer.

TABLE OF CONTENTS

LIST OF TABLES

LIST OF FIGURES

ABSTRACT

This work utilized Pointwise and Fluent to generate a two-dimensional axisymmetric model a Mk 48 torpedo, with the intention of informing methods to reduce the turbulence, and therefore hydrodynamic noise, of the torpedo's wake. However, this work was unable to gather data on the unsteady nature of the turbulence expected around the torpedo due to Fluent providing unrealistic results when run using a transient solver. This work shows that the transient solver computed boundary layers greater than one order of magnitude smaller than expected, and in some cases there was no change in boundary layer thickness over the torpedo's body. The work does contain steady state solutions that were validated by first performing a grid convergence study for a flat plate. The steady state results for the flat plate and torpedo both showed the expected growth for a turbulent boundary layer. Additionally, there was a high level of convergence with the Log-Law showing that the steady state data is valid. Future work should use a transient solver to determine the characteristics of the turbulence to resolve unsteady flow from vortex shedding, wake characteristics, and any broadband or narrowband noise to develop solutions to reduce the noise made by the Mk 48.

Keywords

Computational Fluid Dynamics, Fluent, Pointwise, Turbulence

1. INTRODUCTION

Stealth is one of the primary characteristics of submarine warfare, sound reduction is a key to successful operations, especially in warfare [1]. Because of this, a submarine's primary weapons must be quiet as well. Mk 48 torpedoes are "the US Navy's most capable and potent anti-surface and anti-submarine weapon[s] in use aboard US Navy and allied submarines today" [2]. This thesis focuses on turbulence analysis of an axisymmetric body based on the size, shape, and speed of a Mk 48 torpedo to calculate turbulent statistics and characteristic flow length scales required to inform noise reduction strategies.

Figure 1 displays a Mk48 torpedo and its four main components. From forward to aft the torpedo has a nose section that is primarily sensors for guidance. Next is the warhead section of the torpedo. Behind it is the guidance and control system. Finally, in the stern of the torpedo is the propulsion equipment and fuel. The most important characteristics of the Mk48 for the purposes of this work are its maximum speed, length, and diameter, which are 14.4 m/s, 5.8m, and 53 cm respectively.

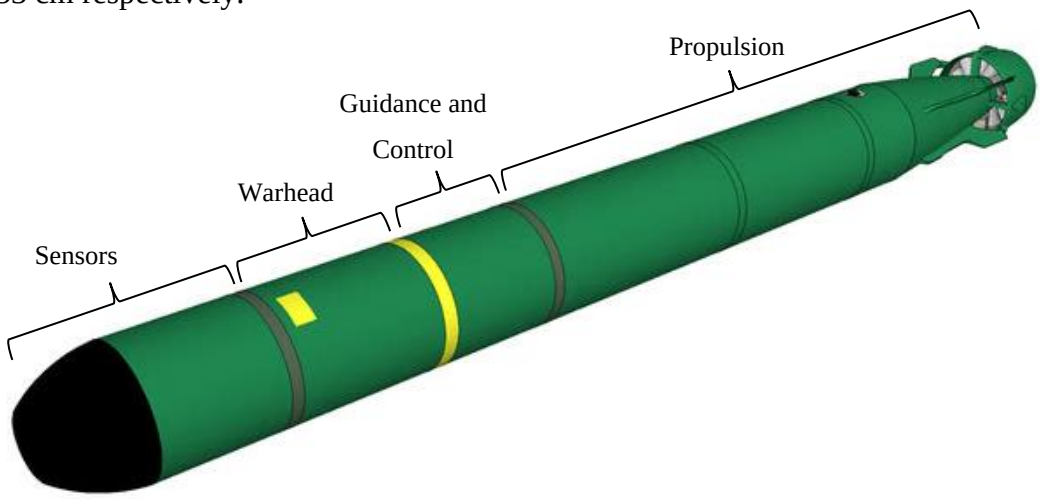

Figure 1. Mk48 ADCAP torpedo [3]

Turbulence creates noise in several common scenarios. A common example is "wind noise" in a car driving on the highway. Reducing turbulent noise in cars has been accomplished by smoothing transitions around the windshield and rearview mirrors [4].

In addition to the noise it creates, flow separation turbulence increases pressure drag. This can effect the maximum speed of a torpedo, which needs to be able to outpace a submarine or

surface that is trying to evade it. According to the Guinness World Records, the fastest military submarine went over 40 knots (20.6 m/s) and surface ships can travel at even greater speeds [5].

Based on the need for faster and quieter torpedoes, a focus on reducing the acoustic and hydrodynamic signatures can improve performance and capabilities of modern torpedoes.

This work makes use of computational fluid dynamics to estimate the turbulent flow characteristics of the boundary layer around the Mk48 torpedo.

2. LITERATURE REVIEW

The basis for the shape and speed of the axisymmetric body tested in this work was the Mk 48 advanced capabilities (ADCAP) heavyweight torpedo. According to the US Navy, this torpedo is used by all submarines for anti-submarine warfare and anti-surface warfare [6]. The Mk 48 ADCAP torpedo recently upgraded the propulsion unit to significantly reduce noise signatures [6]. Both the manufacturer and US Navy state that the torpedo travels at speeds greater than 28 knots (14.4 m/s), which was the basis for the speed used in this work [2], [6].

There are numerous methods to reduce noise from an object traveling in fluid. In the case of ships, submarines, and other maritime objects, these methods focus on the reduction of noise from the flow noise over the object or the noise created by the propeller.

Methods to control flow noise over an object are often performed by changing the design or shape of the body and improving the smoothness of the material to reduce flow noise. This can be seen in examples similar to reducing noise from car review mirrors by smoothing the transition between the body of the car and the mirror [4]. However, flow noise can also be reduced by controlling the flow over the body as shown in the work by Angland *et al.*, who found that blowing used to change the wakes and adjust the interaction of upstream flow made a significant difference in the level of broadband noise created [7]. The results of this study showed that there was over a 3 dB reduction in noise, which means sound intensity was reduced to less than half of the initial value and for some tests, peak noise was reduced by over 15 dB showing that noise was reduced to less than 1/32 of the original value[7].

In the work of Lee *et al.*, the team studied the noise caused by excitation of a ship's hull due to cavitation of a propeller [8]. In this work, Lee *et al.* used air bubbles to create a boundary between the ship's hull and the propeller, which reduced hull excitation by 75% [8]. In a similar effort, Lee *et al.* used an "air-filled rubber membrane" instead of bubbles [9].

For propeller noise, Bagheri *et al.* tested the use of a coating on a propeller to delay the onset of, and reduce the noise from, cavitation [10]. Meanwhile, Aktas *et al.* tested holes placed at the outer region of propellers to relieve pressure and reduce cavitation [11]. Aktas *et al.* found that this method could reduce cavitation related noise by up to 17 dB with only a 2% reduction in propeller efficiency [11].

In the case of a torpedo, there can also be noise associated with the propeller shroud. Although not simulated in this work, follow on work reviewing the turbulence related to the propeller and its shroud may have similar findings to the work of Dhamankar *et al.* [12]. In this work, Dhamankar *et al.* found that adding chevrons to an aircraft jet engine, they were able to reduce the low frequency noise at the cost of increasing high-frequency noise [12]. In the case of torpedoes this may be an acceptable tradeoff depending on how much the intensity of high frequency noise increases as higher frequency noise attenuates faster, which makes low frequency noise a larger concern.

3. METHODOLOGY

3.1 Flat Plate Mesh Convergence Study

The first step was to simulate the flow over a flat plate geometry with the same computational setup that would be employed for the torpedo calculations.

All meshes were created in Pointwise. To ensure consistency and accurate comparison between the flat plate and torpedo geometries, the methodology for creating the meshes as well as the initial y+ and mesh growth rates were identical.

Pointwise's normal extrusion function was used to build each mesh. This ensured a high level of wall orthogonality, which is critical for Fluent's performance [13]. The boundary conditions for the extrusion were "constant y" to allow the flat plate to be run with a symmetric boundary condition up and downstream of the plate similar to the torpedo's axis boundary conditions. A comparison of the settings used for each mesh and the resulting mesh densities are shown in Table 1. The flat plate started at x=3.048 m and ended at x=8.900 m to be the same length as the torpedo geometry.

Table 1. Flat plate mesh generation settings

Mesh	Dimension spacing	Initial delta s	Initial y+	Growth Rate	Height Stop Condition	Points	Cells	Total Volume (m^3)	Point Density*
1	1.00E-02	1.00E-06	4.82E-01	1.1	5	81006	80282	5.31E+01	1.52E+03
2	6.67E-03	6.67E-07	3.21E-01	1.067	5	178437	177356	5.14E+01	3.47E+03
3	4.44E-03	4.44E-07	2.14E-01	1.044	5	312320	310992	5.63E+01	5.55E+03
4	3.92E-03	3.92E-07	1.89E-01	1.039	5	351232	349866	5.56E+01	6.32E+03

Boundary conditions used for the flat plate are shown in Figure 2. The inlet boundary condition, denoted in green, was set with a streamwise velocity of 14.4 m/s. The flat plate was set as a no slip wall boundary condition. The boundaries in front of and behind the plate the boundary conditions were set to symmetry to simulate the freestream condition. The symmetry boundary condition was analogous to the axis boundary condition that would be used for the torpedo. This maintained consistency in the methodology even though the flat plate required the planar solver while the torpedo used the axisymmetric solver. Finally, the outlet conditions

required minor adjustments to the direction for backflow prevention. This setting was adjusted to have backflow designated as the -x direction.

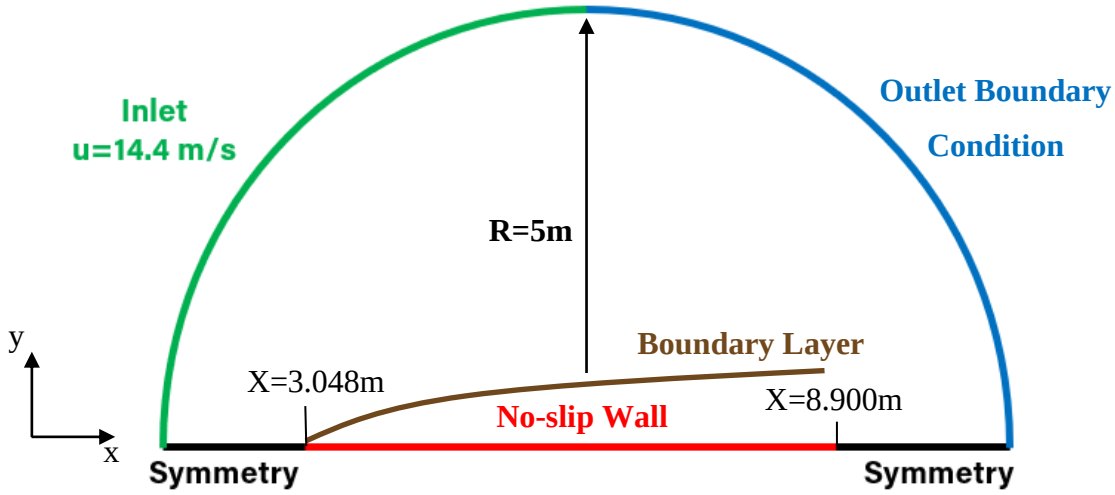

Figure 2. Computational setup for flat plate simulations

The initial mesh convergence study was run using a transient model, similar to initial torpedo simulations. These simulations had a high level of convergence in Fluent's residuals when stepping through time. However, the results did not converge with the expected boundary layer thickness distribution over a flat plate. In fact, the boundary layer thickness did not vary with streamwise location on the plate, even though all four meshes converged to the same boundary layer profile and thickness. Table 2 shows the error between expected and calculated boundary layer thickness at four locations along the flat plate had an error of approximately two orders of magnitude and did not vary with streamwise location on the flat plate. Additionally, Figure 3 shows Fluent's residuals from the baseline mesh using the transient, laminar solver. This shows that Fluent believed there was a high level of convergence, even with the errors in boundary layer thickness.

Table 2. Comparison between expected boundary layer thickness at various x locations and results from transient, laminar fluent calculations on various mesh resolutions for a flat plate

Type of Calculation	Mesh	BL Height X=0.95 m	BL Height X=1.95 m	BL Height X=2.95 m	BL Height X=3.95 m
Expected - laminar		1.29E-03	1.84E-03	2.27E-03	2.62E-03
Transient, laminar Fluent calculation	1	1.85E-05	1.85E-05	1.85E-05	1.85E-05
	2	9.09E-06	9.09E-06	9.09E-06	9.09E-06
	3	6.11E-06	6.11E-06	6.11E-06	6.11E-06
	4	4.68E-06	4.68E-06	4.68E-06	4.68E-06

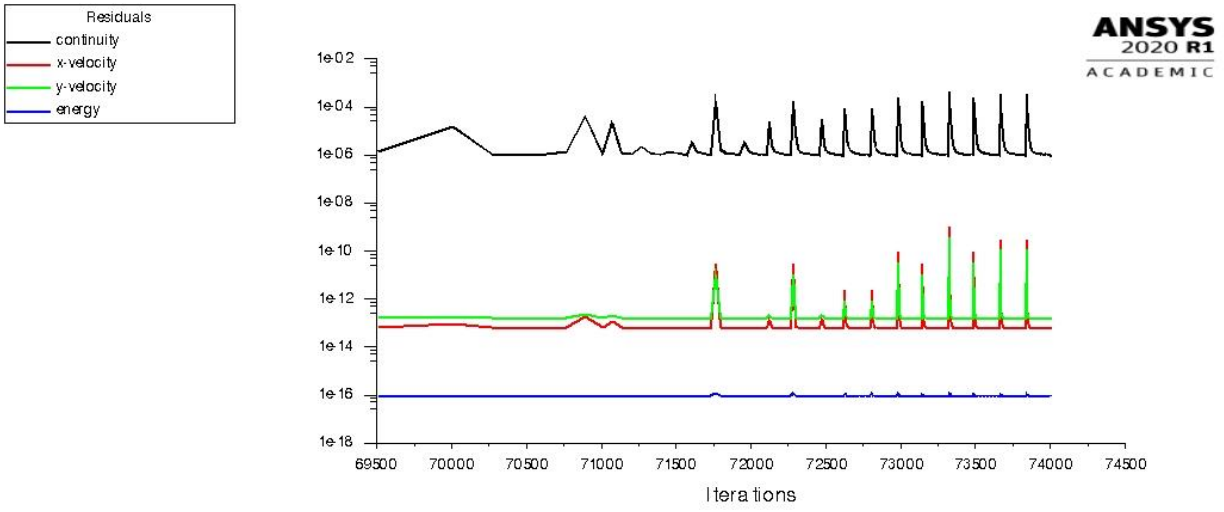

Figure 3. Fluent residuals for the baseline grid (mesh 1) from transient, laminar calculations

Figure 4 depicts Fluent converging on a boundary layer profile – as the grid is refined the change in the boundary layer shape reduces. As shown, the shape of the boundary layer appears to be a laminar profile, but the magnitude error and constant boundary layer thickness at different streamwise locations are evident.

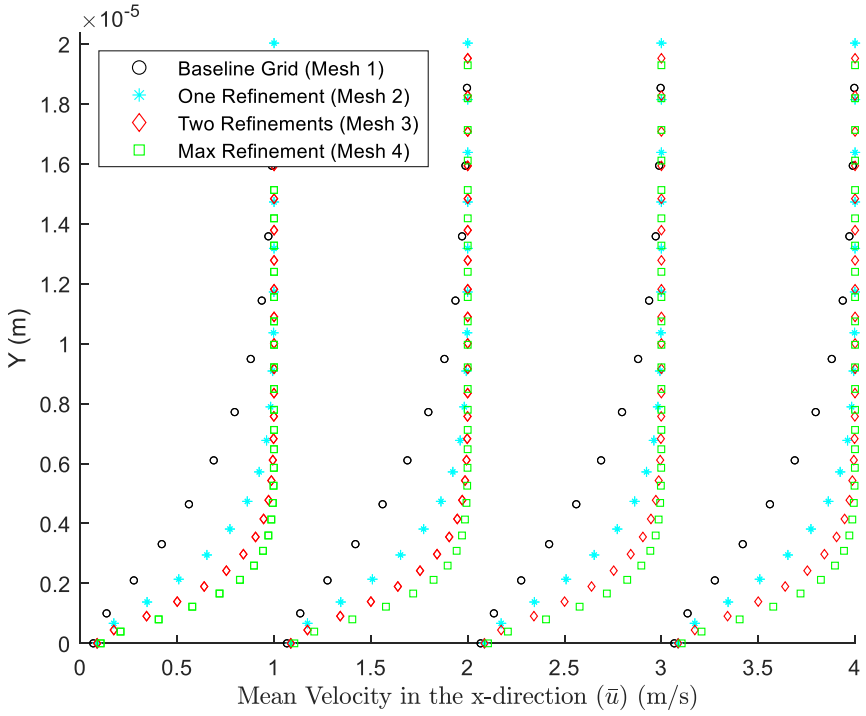

Figure 4. Streamwise velocity profiles at various x locations from transient, laminar flat plate calculations for various mesh resolutions

Figure 5 displays the boundary layer thickness as a function of streamwise location on the flat plate. The data showed a small step increase in the first few data points, however, the overall profile shows a constant boundary layer thickness that is not found in experimental data. Turbulent calculations provided similar results, but had slightly thicker boundary layers.

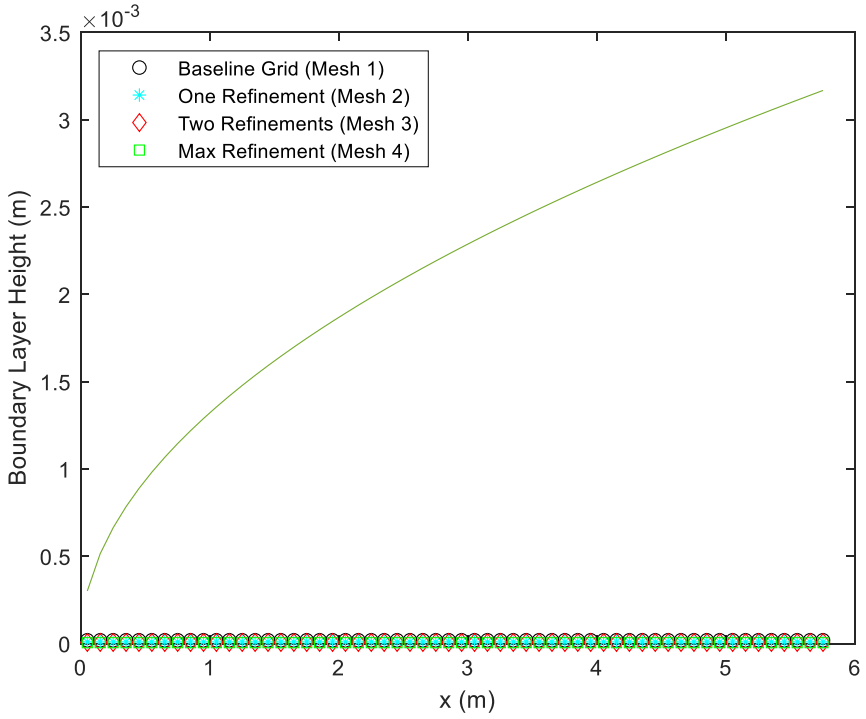

Figure 5. Boundary layer thickness vs. streamwise location from transient, laminar flat plate calculations for various mesh resolutions comparing Fluent calculations with expected

When rerun as a steady state simulation, Fluent residuals did not converge. In fact, for all four meshes the laminar simulation did not converge below residual levels of 100. When using a turbulent model (k-ω), some solutions converged below the default threshold Fluent values, which are 10^{-3} for all except energy which is 10^{-6}. To ensure consistency in the results, simulations were allowed to run until residuals did not change with additional iterations.

The steady state simulations with both laminar and k-ω models showed a high degree of convergence. This is true in terms of grid convergence (similar to transient results show in Figure 4) and convergence to the expected boundary layer profile over a flat plate shown in Eq 1 and Eq 2 for laminar and turbulent boundary layers respectively.

$$\delta_{99,lam}(x) \cong 5.0\sqrt{\frac{\nu x}{u_0}} = 5.0\frac{x}{\sqrt{Re_x}} \tag{1}$$

$$\delta_{99,turb}(x) \cong 0.37\frac{x^{4/5}}{\left({u_0}/{\nu}\right)^{1/5}} = 0.37\frac{x}{{Re_x}^{1/5}} \tag{2}$$

Table 3 displays the expected and computed boundary layer thickness and four discrete locations along the flat plate for all four meshes using a laminar and turbulent solver. These results show a high level of convergence with the expected results. For the laminar cases, the largest percent error is seen in the coarsest mesh at X=3.95 m and equates to 7% error. However, all three of the refined meshes have an error of 3% or less at all four locations. Additionally, the variance for the laminar case is on the order of 10^{-9} or less at all four locations, which shows the solutions are distributed closely around the expected values.

In the turbulent calculations, the largest error is 13% and is found in the most refined mesh at X=0.95 m. The location X=0.95 m had the highest error for all four meshes and this value was consistent with those found in the coarse meshes, as shown by the variance being on the order of 10^{-6}. Based on these results, it is clear that Fluent produces higher quality results when using the steady state solver for the flat plate boundary layer calculations.

Table 3. Comparison between expected boundary layer thickness at various x locations and results from steady state, laminar and k-ω fluent calculations on various mesh resolutions for a flat plate

Type of Calculation	Mesh	BL Height X=0.95 m	BL Height X=1.95 m	BL Height X=2.95 m	BL Height X=3.95 m
Expected - laminar		1.29E-03	1.84E-03	2.27E-03	2.62E-03
Steady state, laminar Fluent calculation	1	1.30E-03	1.90E-03	2.30E-03	2.80E-03
	2	1.30E-03	1.90E-03	2.30E-03	2.60E-03
	3	1.30E-03	1.80E-03	2.30E-03	2.60E-03
	4	1.30E-03	1.80E-03	2.30E-03	2.60E-03
Expected - turbulent		1.32E-02	2.34E-02	3.26E-02	4.12E-02
Steady state, k-ω Fluent calculation	1	1.16E-02	2.26E-02	3.34E-02	4.41E-02
	2	1.16E-02	2.26E-02	3.31E-02	4.41E-02
	3	1.18E-02	2.25E-02	3.32E-02	4.30E-02
	4	1.15E-02	2.20E-02	3.23E-02	4.23E-02

In addition to the statistic based analysis discussed above, a visual check was performed for the boundary layer shape (Figure 6 and Figure 8) and thickness (Figure 7 and Figure 9) for each case described in Table 3. These figures clearly show the expected boundary layer profiles for a laminar and turbulent boundary layer as well as a high level of convergence with the expected boundary layer thickness over the entirety of the flat plate.

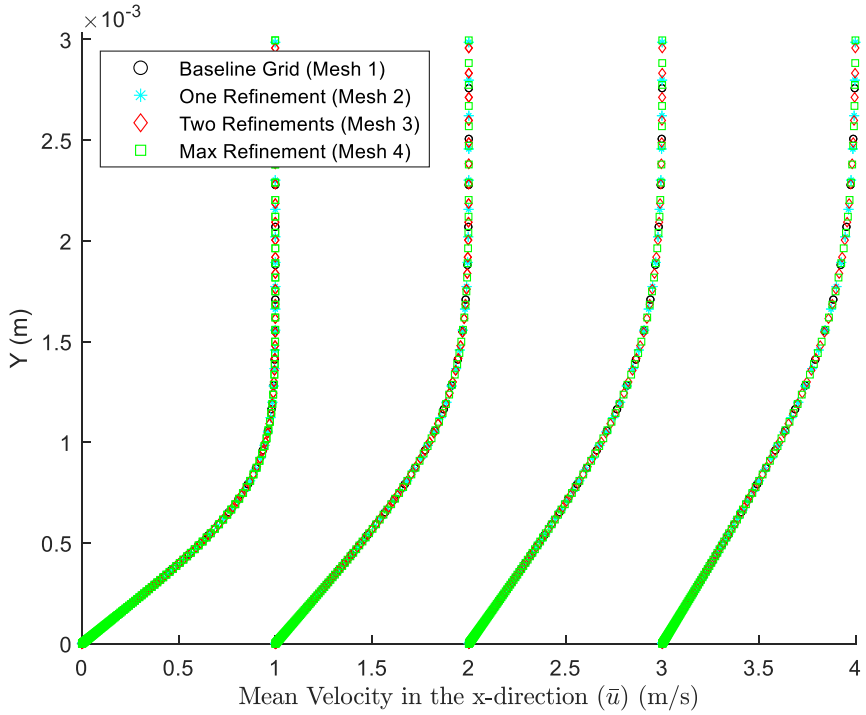

Figure 6. Streamwise velocity profiles at various x locations from steady state, laminar flat plate calculations for various mesh resolutions

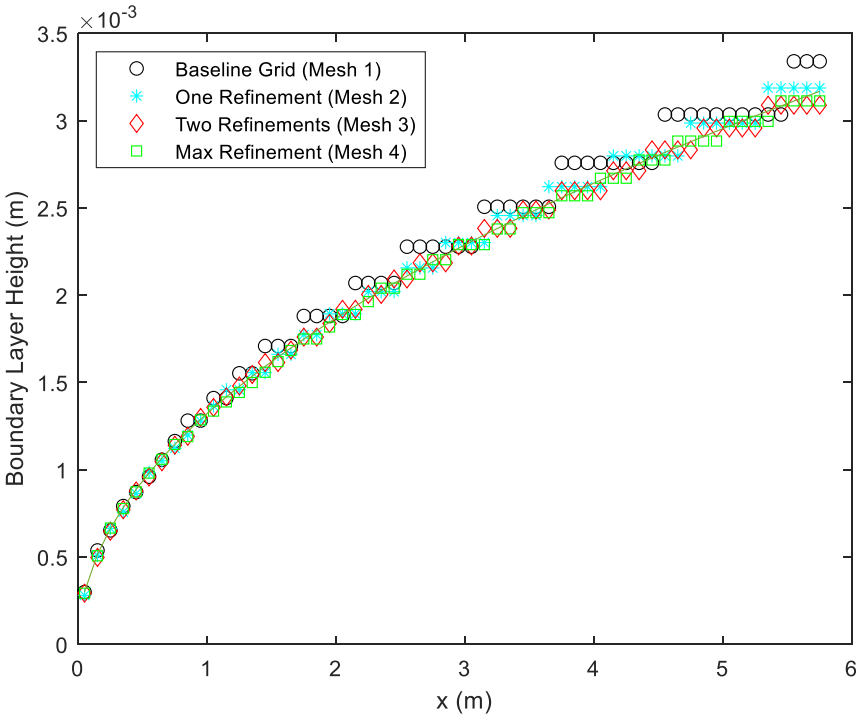

Figure 7. Boundary layer thickness vs. streamwise location from steady state, laminar flat plate calculations for various mesh resolutions comparing Fluent calculations with expected

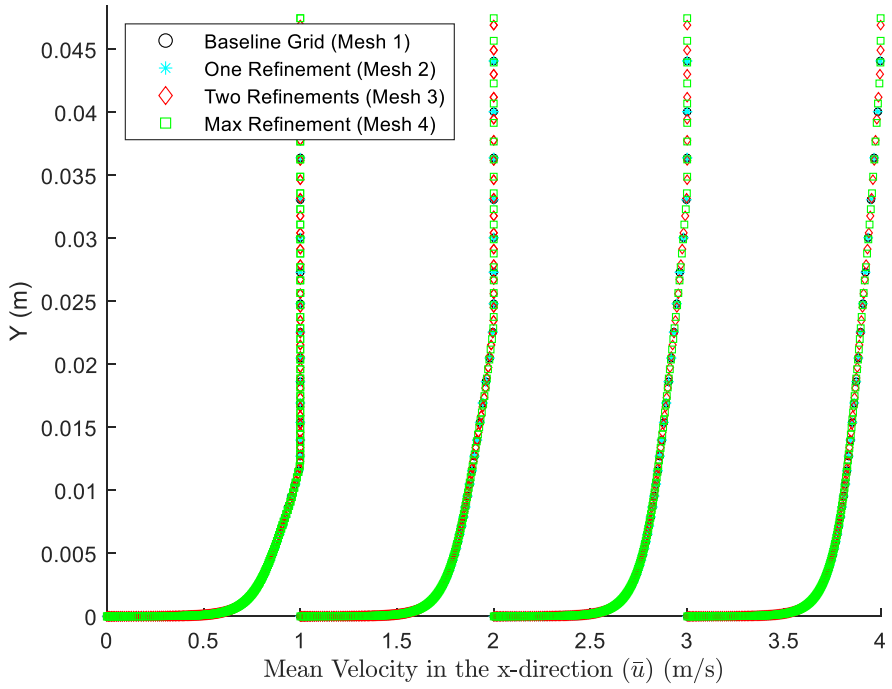

Figure 8. Streamwise velocity profiles at various x locations from steady state, k-ω flat plate calculations for various mesh resolutions

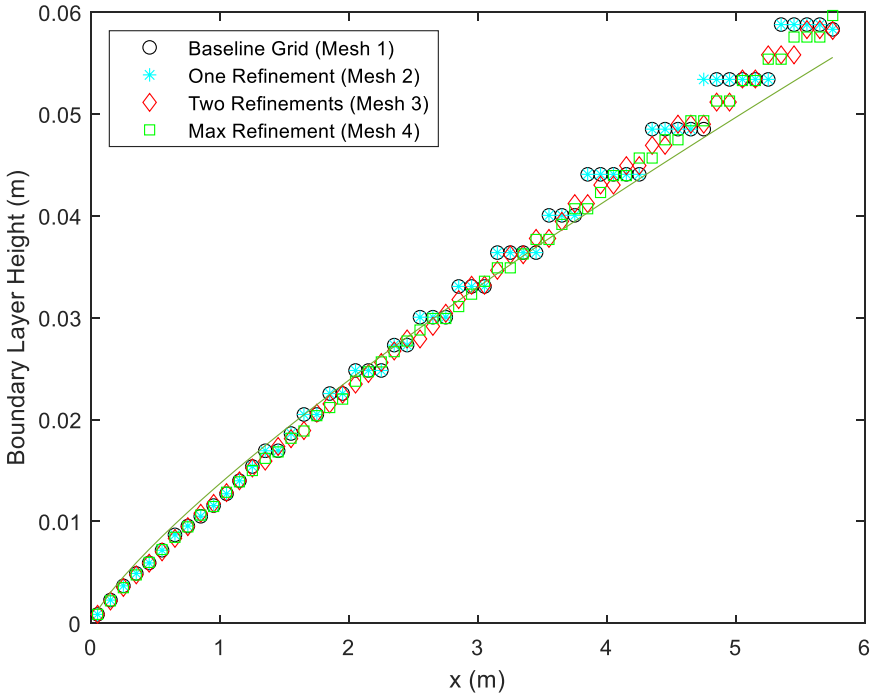

Figure 9. Boundary layer thickness vs. streamwise location from steady state, k-ω flat plate calculations for various mesh resolutions comparing Fluent calculations with expected

Based on Fluent's transient calculations producing results far from the expected boundary layer thickness, even with high levels of residual convergence, all follow-on work with the torpedo geometry was calculated using Fluent's steady state solver. While using the steady state solver, calculations ran until Fluent residuals held constant to ensure the solution was accurate.

3.2 Torpedo Mesh Convergence Study

To continue a grid convergence study for the torpedo geometry, four torpedo meshes were run with a steady state model in ANSYS Fluent [13].

The shape of the torpedo studied was based on a Mk 48 torpedo 3D Computer Aided Design (CAD) file available online [3]. The geometry was simplified to run the CFD simulations as 2D axisymmetric problems. The points used to create the geometry are shown below in Table 4.

Table 4. Points used to create the torpedo geometry

Point	x (m)	y (m)	x (ft)	y (ft)
p1	3.048	0.000	10	0
p2	3.048	0.107	10	0.35
p3	3.170	0.201	10.4	0.66
p4	3.383	0.259	11.1	0.85
p5	7.620	0.259	25	0.85
p6	8.900	0.046	29.2	0.15
p7	8.900	0.000	29.2	0

The initial y+ and growth rate settings for the torpedo meshes are identical to the flat plate meshes. These values and the resulting mesh densities can be seen in Table 5.

Table 5. Torpedo mesh generation settings

Mesh	Dimension spacing	Initial delta s	Initial y+	Growth Rate	Height Stop Condition	Points	Cells	Total Volume (m^3)	Point Density*
1	1.00E-02	1.00E-06	4.82E-01	1.1	5	84042	83296	9.91E+02	8.48E+01
2	6.67E-03	6.67E-07	3.21E-01	1.067	5	185339	184224	1.11E+03	1.67E+02
3	4.44E-03	4.44E-07	2.14E-01	1.044	5	418155	416480	1.14E+03	3.66E+02
4	3.92E-03	3.92E-07	1.89E-01	1.039	5	511756	509922	1.12E+03	4.57E+02

Boundary conditions used for the torpedo are similar to those from the flat plate calculations and are shown in Figure 10. The inlet boundary condition was set with a streamwise velocity of

14.4 m/s based on the top speed [2]. The torpedo's body was set as a no-slip wall boundary condition. In front of and behind the torpedo the boundary conditions were set to axis boundary conditions allowing for the axisymmetric rotation. Like the flat plate, the outlet conditions required minor adjustments to the direction for backflow prevention and used the -x direction for the backflow condition.

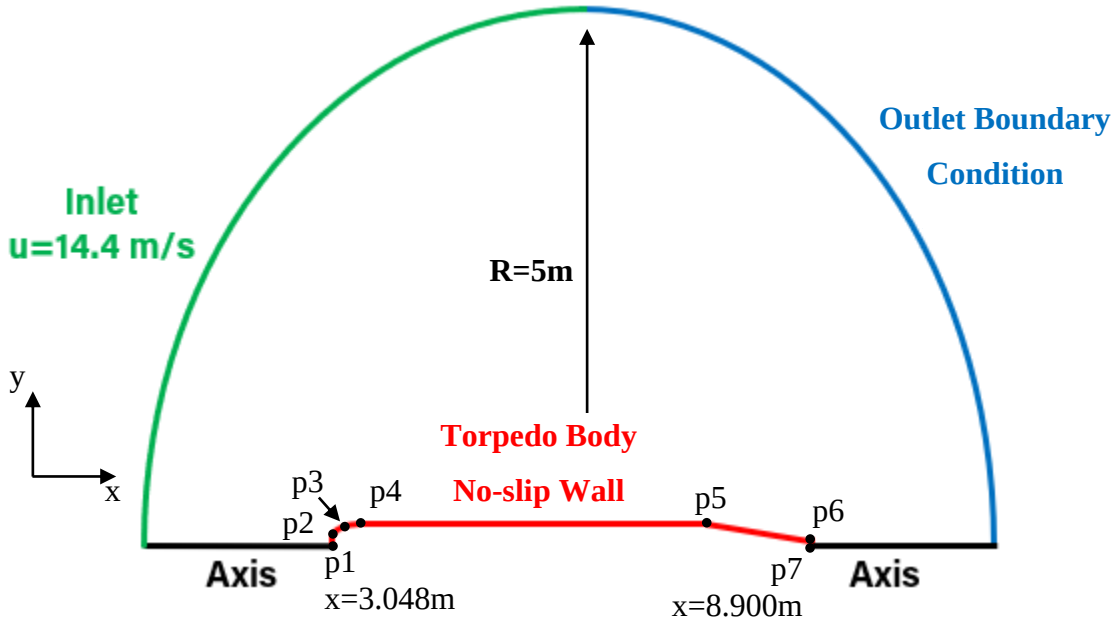

Figure 10. Computational setup for torpedo simulations

The torpedo geometry was run using a laminar solver. However, Fluent residuals did not achieve a steady-state solution as seen on the flat plate simulations. Instead, the residuals fluctuated in a small band and the resulting velocity contours displayed results that appear unphysical. The resulting axial velocity contour can be seen in Figure 11. Based on the residuals and resulting velocity contours, the torpedo grid convergence was run using a turbulent model.

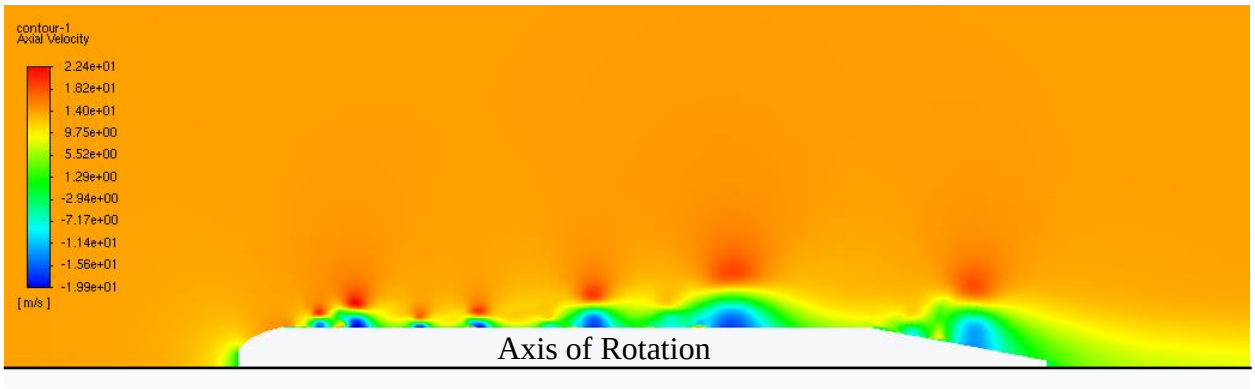

Figure 11. Non-converged numerical solution from Fluent steady-state, laminar solver showing axial velocity contours over torpedo geometry

Table 6 shows the boundary layer thickness of the torpedo at four discrete locations. All four locations are on located where the torpedo's radius is largest and constant to ensure the data used in perpendicular to the torpedo's body. While this is an axisymmetric problem and the flat plate boundary layer thickness is not expected to be an exact estimate of the solution, it does provide a reference for the expected order of magnitude and growth rate of the boundary layer thickness. In this case, the highest percent difference from the expected flat plate boundary layer thickness was 12% and the variance compared to the flat plate was on the order of 10^{-6}. When comparing the four meshes with their mean, the variance was on the order of 10^{-7}. These statistics show a high level of convergence among the different mesh densities and clearly show that all four mesh densities are sufficient for use in subsequent calculations.

Table 6. Comparison between expected boundary layer thickness at various x locations and results from steady state, k-ω fluent calculations on various mesh resolutions for a torpedo

Type of Calculation	Mesh	BL Height X=0.95 m	BL Height X=1.95 m	BL Height X=2.95 m	BL Height X=3.95 m
Expected - turbulent		1.32E-02	2.34E-02	3.26E-02	4.12E-02
Steady state, k-ω Fluent calculation	1	1.40E-02	2.49E-02	3.65E-02	4.43E-02
	2	1.33E-02	2.40E-02	3.54E-02	4.31E-02
	3	1.28E-02	2.46E-02	3.47E-02	4.31E-02
	4	1.27E-02	2.44E-02	3.45E-02	4.34E-02

In addition to the statistical analysis, a visual review was performed to ensure the turbulent boundary layer had the expected shape and that the boundary layer grew at the correct rate. Figure 12 shows that the four locations evaluated in Table 6 display the expected turbulent boundary layer profile. Additionally, Figure 13 indicates a high level of convergence in the growth of the boundary layer thickness between all four mesh densities. The boundary layer thickness grows more quickly than expected by the flat plate equation, but it is possible that this is due to the up or downstream geometry and its effects on the boundary layer. There are two outliers in the data for the coarsest mesh near the end of the data reviewed. These two points are circled in orange as the boundary layer thickness increases and then decreases back to the previous value. It is possible that the coarsest mesh begins to display the effects of the downstream geometry as the torpedo diameter reduces in the tail section or that there is a minor divergence in the solutions. For the first possibility, a consistent reduction in boundary layer thickness was seen in the axial velocity contour plots as the tail section of the torpedo was approached. Figure 14 displays an overall contour of the torpedo's axial velocity and a subset focused on the change in geometry as the radius begins to reduce in the tail section to show the effect on boundary layer thickness.

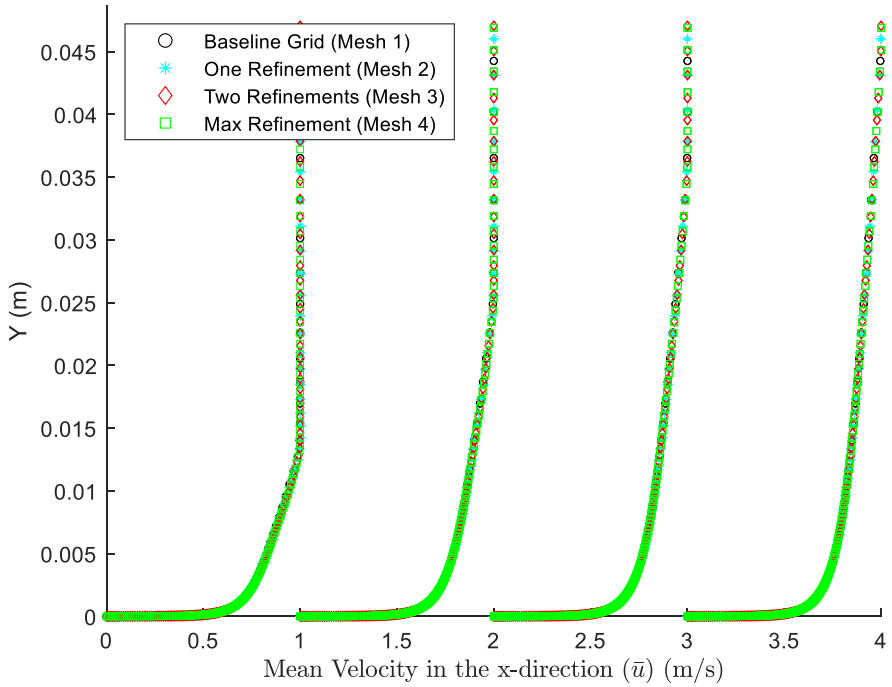

Figure 12. Streamwise velocity profiles at various x locations from steady state, k-ω torpedo calculations for various mesh resolutions

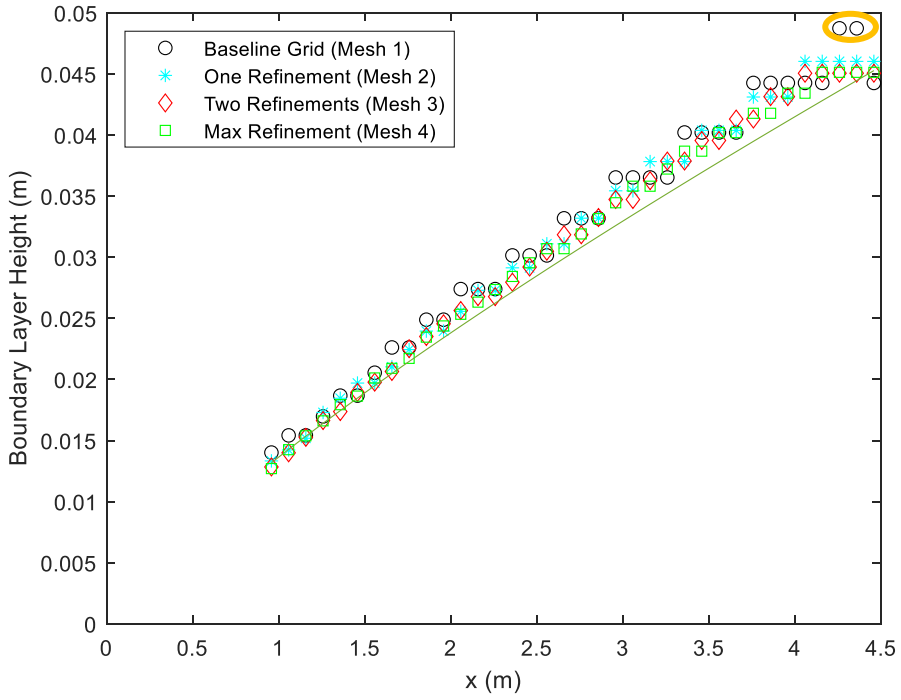

Figure 13. Boundary layer thickness vs. streamwise location from steady state, k-ω torpedo calculations for various mesh resolutions comparing Fluent calculations with expected

Figure 14. Boundary Layer Thickness Reduction due to Torpedo Tail Geometry

3.3 Torpedo non-dimensional Results Convergence Study

After confirming that the grid used in this work was sufficient for solution convergence using Fluent's steady state k-ω solver, additional review of the boundary layer was performed to ensure convergence with the expected turbulent boundary layer in terms of y+ and u+. The u+ and y+ values were calculated using Eq 3 through Eq 5.

$$u_\tau = \sqrt{\frac{\tau_w}{\rho}} \tag{3}$$

$$y^+ = \frac{y u_\tau}{\upsilon} \tag{4}$$

$$u^+ = \frac{u}{u_\tau} \tag{5}$$

As shown in Figure 15, the simulation results for the most refined mesh strongly agree with the expected Law of the Wall and Log-Law shown in Eq 6. Table 7 lists the best fit lines through the log-law region at each location in the form of the log-law equation. These values were

calculated by finding the best fit through y+ and u+ values between u+ of 13 and 19. These characteristics are additional confirmations that the mesh convergence is high.

$$u^+ = \frac{1}{\kappa} ln(y^+) + C^+ \tag{6}$$

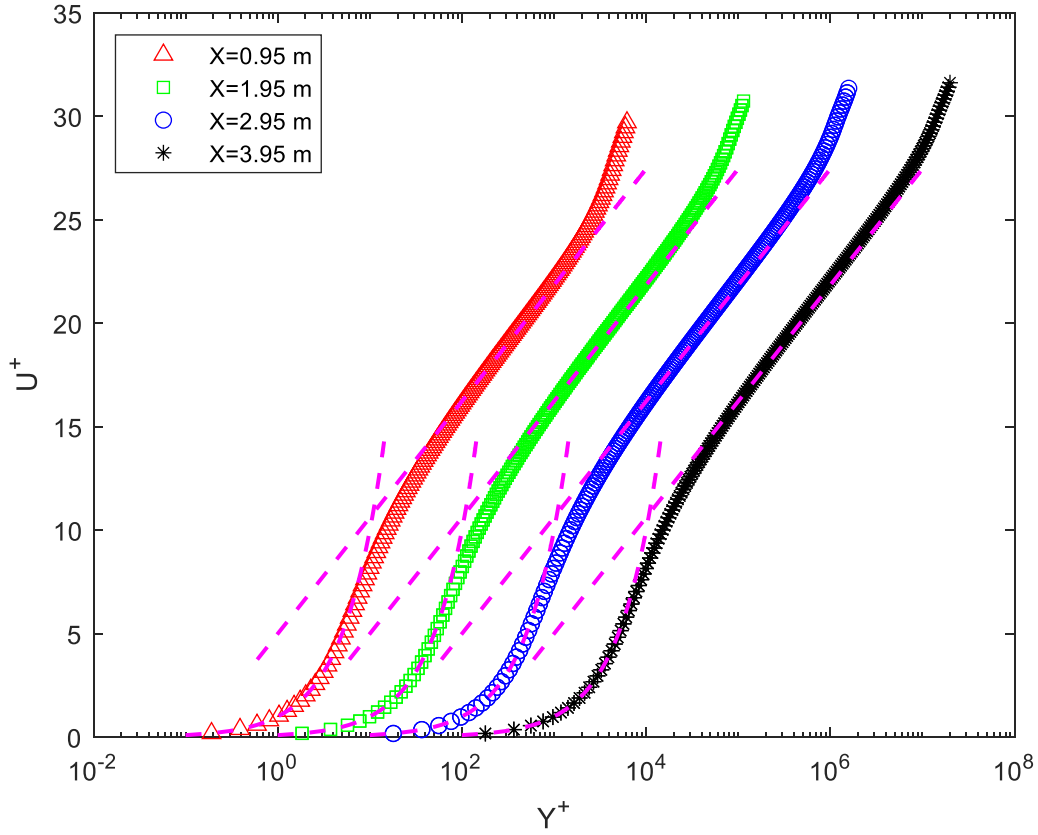

Figure 15. Non-dimensional streamwise velocity profiles at various x locations from steady state, k-ω torpedo calculations on the max refinement mesh (mesh 4) compared to the Law of the Wall and Log-Law

Table 7. κ and C values at various x locations from steady state, k-ω torpedo calculations on the max refinement mesh (mesh 4) compared to the classical Log-Law values

Location (m)	C+	κ
0.95	2. 775	0.301
1.95	2. 777	0.302
2.95	2. 777	0.302
3.95	2.778	0.302
Classic Values	5	0.410

4. RESULTS AND DISCUSSION

4.1 Turbulent Shear Stress Results from the Steady State Solution

The most refined steady state solution was studied to see what other data could be useful for informing future work and reducing the torpedo's turbulence and noise. Turbulent shear stress was the primary focus and it was calculated as

$$\tau_t = \nu_t \frac{\partial u}{\partial y}, \tag{7}$$

where ν_t is the turbulent viscosity. The turbulent shear stress profiles at four discrete locations on the torpedo body are shown in Figure 16. These profiles are the correct shape for a wall bounded flow. Further analysis of these profiles and their implications is recommended in future work.

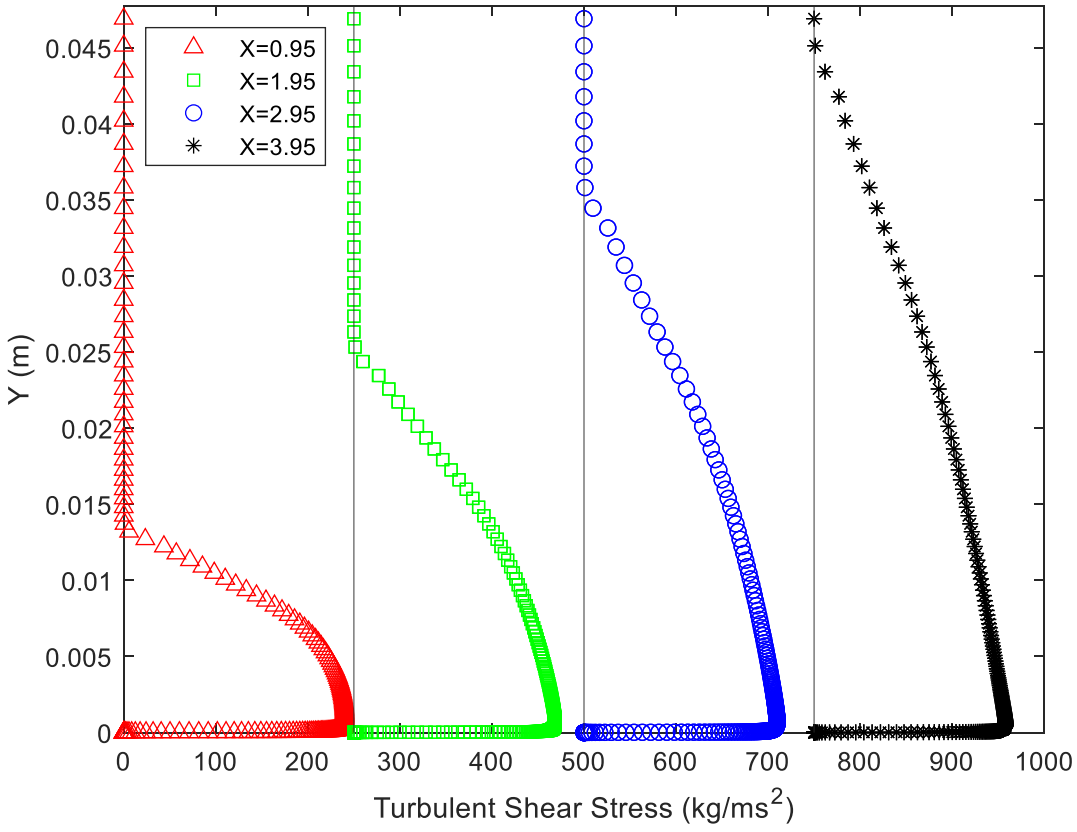

Figure 16. Turbulent Shear Stress Profiles at various x locations from steady state, k-ω torpedo calculations on the max refinement mesh (mesh 4)

4.2 Attempt to simulate flow unsteadiness in the torpedo's wake

To determine more quantitative information about the turbulence and wake generated by a torpedo, the baseline mesh (mesh 1) tested in the grid convergence study was split into two sections. This was meant to focus computational resources at the aft end of the torpedo. The upstream, or forward, portion of the torpedo was run using a steady state solver and its "outlet" conditions were used as the inlet to the downstream, or aft, portion of the torpedo simulation. A diagram of this geometry can be seen in Figure 17.

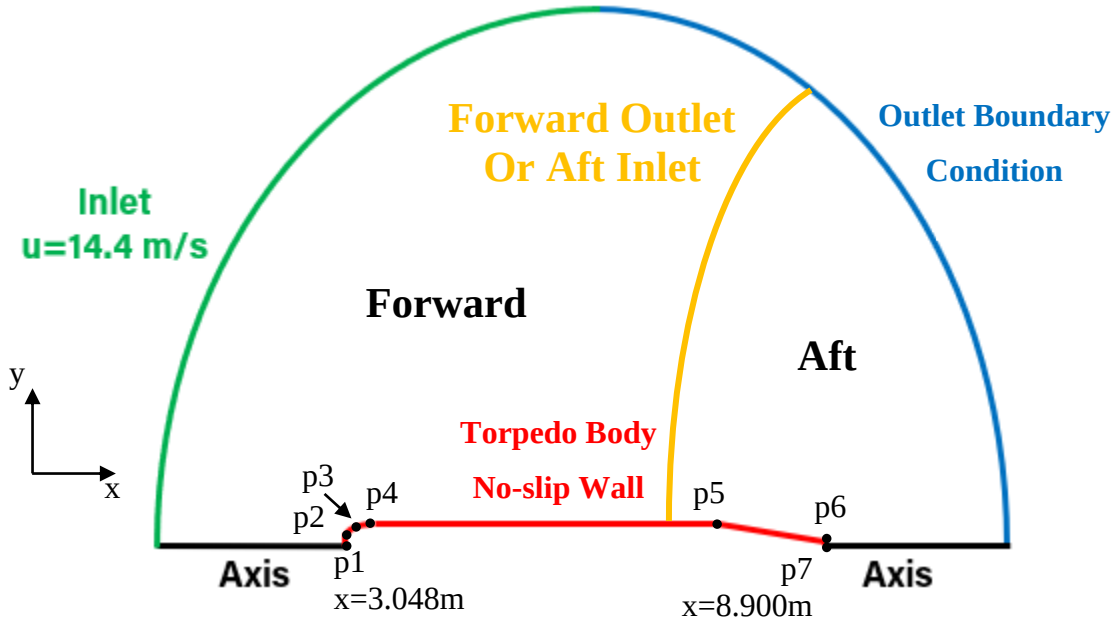

Figure 17. Computational setup for split torpedo

The initial split location of the mesh was used was determined to be too far downstream when the velocity contours of the split mesh were compared to the results in the grid convergence study. This difference was caused due to the upstream propagation of the effects of the torpedo geometry, specifically the necking down of the radius in the torpedo's tail section. The location of the split in the mesh was improved by viewing a contour displaying the difference in the axial velocity between the full and split mesh.

After improving the split location, a review of the boundary layer shape and boundary layer thickness over streamwise locations was performed and shows that there is a high level of convergence between the full and split mesh. These results can be seen in Figure 18 and Figure 19.

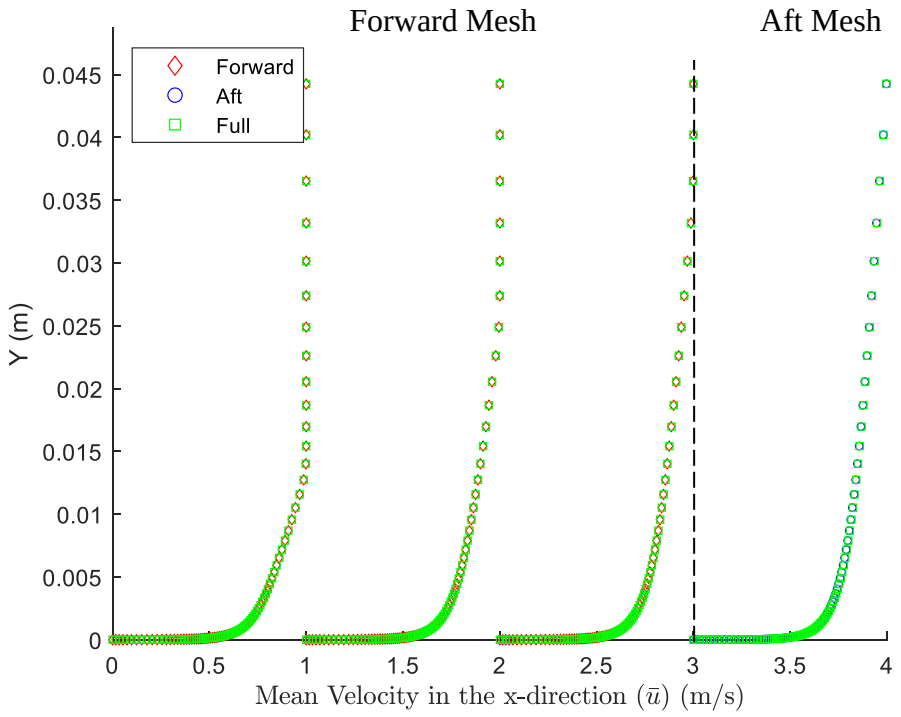

Figure 18. Streamwise velocity profiles at various x locations from steady state, k-ω torpedo calculations on a split and full mesh

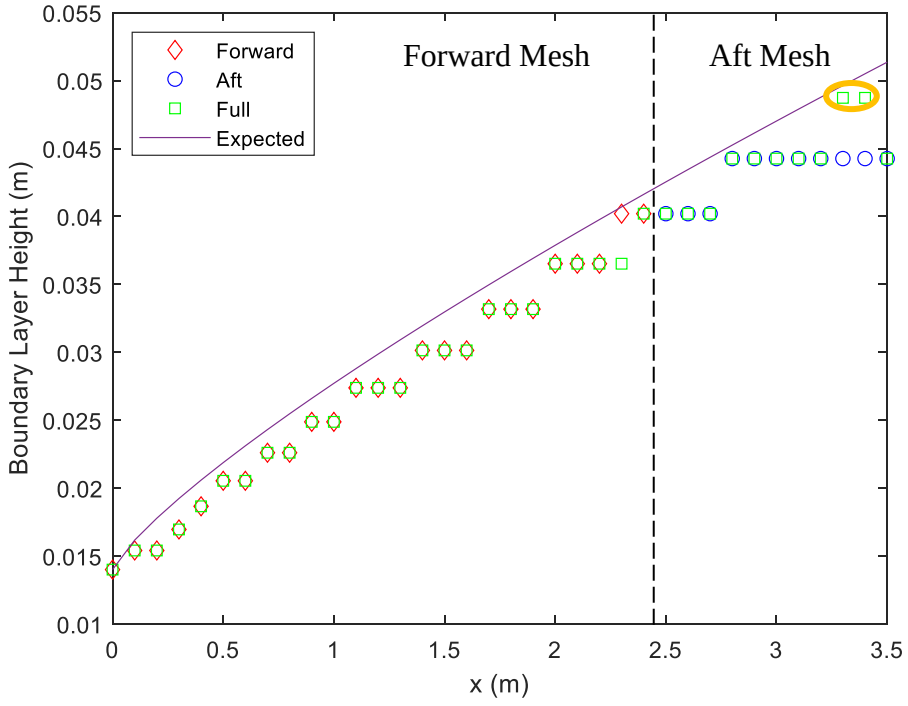

Figure 19. Boundary layer thickness vs. streamwise location from steady state, k-ω torpedo calculations on a split and full mesh comparing Fluent calculations with expected

The difference in contours was also resulted in satisfactory level of similarity in the steady state solution shown by the difference is the axial velocity contour in Figure 20. The largest difference in the solution is 0.4 m/s, which is 3% of the inlet axial velocity.

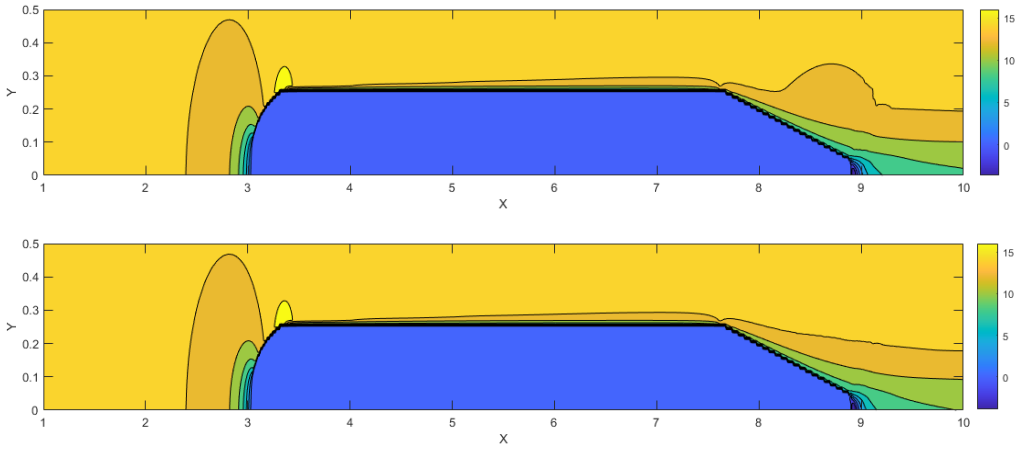

Figure 20. Streamwise velocity contours from steady state, k-ω torpedo calculations on a split (top) and full (bottom) mesh

The aft portion of the mesh was run in a transient setting to determine if there was unsteadiness in the flow that could be evaluated. This was performed using both a k-ω model as well as a Detached Eddy Simulation (DES) model. However, no unsteadiness was observed.

To determine if it was due to the inlet conditions being based on a steady solution, the DES model was used to insert fluctuations at the inlet of the aft mesh. This was performed using the upstream, steady state solution for turbulent kinetic energy (TKE). These results did not display any temporal unsteadiness when extracting probe data in CFD Post and viewing the change in axial velocity, radial velocity, or vorticity. Additionally, viewing the contours of these parameters throughout time did not display a significant spatial variation so a proper orthogonal decomposition was not attempted either.

Considerations were made that the TKE from the steady state solution may have underestimated the turbulence and the inlet conditions were shifted to use turbulent intensity and was run at values of 3%, 10%, and 20%. None of these levels propagated the unsteadiness. In fact, the unsteadiness viewed at the inlet was damped out by the time it reached the change in radius at the torpedo's tail section.

This work was unable to determine if the lack of unsteadiness and reduction of fluctuations was due to the errors in Fluent's transient calculations displayed in the grid convergence studies or due to the design of the torpedo's geometry.

5. CONCLUSION

This work was unable to determine the characteristics of a torpedo's wake and related turbulence based on the quality of transient data computed. However, this work was able to verify the methodology and convergence of steady state turbulent solutions for an axisymmetric 2D simulation of a Mk 48 torpedo.

It is recommended that this work be continued to properly compute the transient data using a corrected model in order to perform temporal and spatial analysis of the wake of a torpedo. Once 2D axisymmetric results are achieved it is recommended that a 3D Large Eddy Simulation or DES model be used to extract the highest quality data to enable design improvements to the Mk 48 torpedo.

REFERENCES

[1] "From attack submarines to spies: US Navy asks more of its underwater fleet." https://www.naval-technology.com/features/us-nuclear-attack-submarines/ (accessed Sep. 13, 2021).

[2] "MK 48 Mod 7 Common Broadband Advanced Sonar System (CBASS) Heavyweight Torpedo." https://www.lockheedmartin.com/en-us/products/mk-48-mod-7-common-broadband-advanced-sonar-system-cbass-heavyweight-torpedo.html (accessed Mar. 16, 2021).

[3] "3D Warehouse." https://3dwarehouse.sketchup.com/model/7c8dc11ee845b14f14621506c22882a0/Mark-48-ADCAP-torpedo?hl=en (accessed Sep. 21, 2021).

[4] Doug Tews, "A Crucial Element Needed For A Truly Quiet Car: Subframes." https://elevatingsound.com/a-crucial-element-needed-for-a-truly-quiet-car-subframes/ (accessed Sep. 13, 2021).

[5] "Guinness World Records." https://www.guinnessworldrecords.com/world-records/fastest-military-submarine (accessed Sep. 18, 2021).

[6] "MK 48 - Heavyweight Torpedo," Dec. 06, 2013. https://www.navy.mil/Resources/Fact-Files/Display-FactFiles/Article/2167907/mk-48-heavyweight-torpedo/ (accessed Mar. 16, 2021).

[7] D. Angland, X. Zhang, and M. Goodyer, "Use of blowing flow control to reduce bluff body interaction noise," in AIAA Journal, Aug. 2012, vol. 50, no. 8, pp. 1670–1684. doi: 10.2514/1.J051074.

[8] J. H. Lee, H. G. Park, J. H. Kim, K. J. Lee, and J. S. Seo, "Reduction of propeller cavitation induced hull exciting pressure by a reflected wave from air-bubble layer," Ocean Engineering, vol. 77, pp. 23–32, Feb. 2014, doi: 10.1016/j.oceaneng.2013.12.007.

[9] J. H. Lee, K. J. Lee, H. G. Park, and J. H. Kim, “Possibility of air-filled rubber membrane for reducing hull exciting pressure induced by propeller cavitation,” Ocean Engineering, vol. 103, pp. 160–170, May 2015, doi: 10.1016/j.oceaneng.2015.04.073.

[10] B. MR, S. MS, and M. H, “An Experimental Study on the Effect of IS700 Coating on the Cavitation Inception and Development, and Noise Reduction of a Marine Propeller,” Journal of Applied Mechanical Engineering, vol. 06, no. 03, 2017, doi: 10.4172/2168-9873.1000267.

[11] B. Aktas, N. Yilmaz, M. Atlar, N. Sasaki, P. Fitzsimmons, and D. Taylor, “Suppression of tip vortex cavitation noise of propellers using pressureporestm technology,” Journal of Marine Science and Engineering, vol. 8, no. 3, Mar. 2020, doi: 10.3390/jmse8030158.

[12] N. S. Dhamankar, G. A. Blaisdell, and A. S. Lyrintzis, “Analysis of turbulent jet flow and associated noise with round and Chevron Nozzles using large Eddy simulation,” 2016. doi: 10.2514/6.2016-3045.

[13] “Ansys Fluent, Release 20.1, Help System, ANSYS, Inc.”